Inorganic Chemistry

Article

pubs.acs.org/IC

Crystal Structure and Bonding in $BaAu_5Ga_2$ and $AeAu_{4+x}Ga_{3-x}$ (Ae = Ba and Eu): Hexagonal Diamond-Type Au Frameworks and Remarkable Cation/Anion Partitioning in the Ae−Au−Ga Systems

Volodymyr Smetana,[†,‡] Simon Steinberg,[†,‡] Nathan Card,[‡] Anja-Verena Mudring,*[,†,‡] and Gordon J. Miller*[,†,§]

[†]Ames Laboratory, U.S. Department of Energy, Iowa State University, Ames, Iowa 50011-3020, United States

[§]Department of Chemistry, Iowa State University, Ames, Iowa 50011-3111, United States

[‡]Department of Material Sciences and Engineering, Iowa State University, Ames, Iowa 50011-2300, United States

Supporting Information

ABSTRACT: Five new polar intermetallic compounds in the Ae−Ga−Au system (Ae = Ba, Eu), $BaAu_5Ga_2$ (**I**), $BaAu_{4.3}Ga_{2.7}$ (**II**), $Ba_{1.0}Au_{4.5}Ga_{2.4}$ (**III**), $EuAu_{4.8}Ga_{2.2}$ (**IV**), and $Eu_{1.1}Au_{4.4}Ga_{2.2}$ (**V**), have been synthesized and their crystal structures determined by single-crystal X-ray diffraction. **I** crystallizes in the orthorhombic crystal system with a large unit cell [Pearson symbol *oP*64; *Pnma*, Z = 8, a = 8.8350(5) Å, b = 7.1888(3)Å, c = 20.3880(7) Å], whereas all other compounds are hexagonal [*hP*24; $P\bar{6}2m$, Z = 3, a = 8.54−8.77(1) Å, c = 7.19−7.24(1) Å]. Both structures contain mutually orthogonal layers of Au_6 hexagons in chair and boat conformations, resulting in a hexagonal diamond-like network. Ae atoms and additional $(Au/Ga)_3$ groups are formally encapsulated by $(Au_6)_2$ distorted hexagonal prisms formed of three edge-sharing hexagons in the boat conformation or, alternatively, lie between two Au_6 hexagons in the chair conformation. The $(Au/Ga)_3$ groups can be substituted by Ae atoms in some of the hexagonal structures with no change to the structural symmetry. Tight-binding electronic structure calculations using linear-muffin-tin-orbital methods on idealized models "$BaAu_5Ga_2$" and "$BaAu_4Ga_3$" show both compounds to be metallic with evident pseudogaps near the corresponding Fermi levels. The integrated crystal orbital Hamilton populations are dominated by Au−Au and Au−Ga orbital interactions, although Ba−Au and Ba−Ga contributions are significant. Furthermore, Au−Au interactions vary considerably along different directions in the unit cells, with the largest values for the hexagons in the boat conformation and the lowest values for those in the chair conformation. **II** revealed that partial substitution of Au atoms in the hexagonal diamond net by a post-transition element (Ga) may occur in this family, whereas the sizes of the $(Au/Ga)_3$ groups and strong Ba−Au covalent interactions allow for their mutual replacement in the voids.

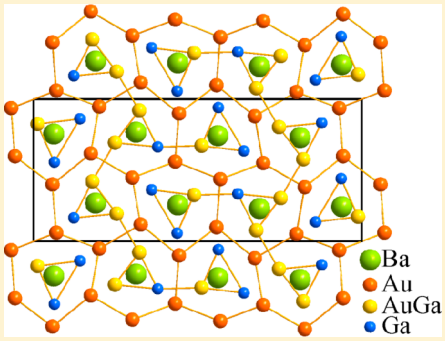

INTRODUCTION

In recent years, many novel polar intermetallic compounds have been discovered.[1] Among the most productive explorations are those including Au with post-transition and active metals. This outcome presumably arises from substantial relativistic effects,[2] leading to enhanced participation of the filled Au 5d orbitals in bonding and larger orbital interactions for Au−Au and Au−heteroatom bonds. In particular, Au, together with Ga or In, has been especially successful in forming ternary compounds with electropositive elements such as Na, K, and Ca because of its electron-accepting, low-lying 6s orbital.[3−7] These compounds exhibit polyanionic frameworks with encapsulated cations forming 1D $(A_{0.55}Au_2Ga_2$ and $AAu_2Ga_4)^4$ or 2D $(AAu_3Ga_2)^3$ tunnels, Au_n clusters,[8] and even a quasicrystal and its crystalline approximants.[6] According to the total valence electron concentrations, such compounds are situated between Hume−Rothery[9] and Zintl phases,[10] to suggest that polar-covalent bonding interactions between anionic and cationic parts might also play an important role in their structural stability. In addition, these compounds exhibit high coordination numbers (16−24) for the electropositive elements and show metallic conductivity, in contrast to Zintl phases, which are typically semiconductors.[11]

Analogous systems involving heavier alkali or alkaline-earth elements have not been systematically investigated, although new structural and unusual cation−anion bonding possibilities exist, especially in compounds with high Au content. In spite of known Au-rich binary phases, i.e., MAu_2 (M = Na, K, Ca, Sr, Ba)[12−15] and MAu_5 (M = K, Rb, Ca, Sr, Ba),[16−18] a very limited number of ternary compounds with Au content approaching, or even exceeding, 50 atomic %, which would allow a larger proportion of Au−Au bonds, has been reported, viz., K_4Au_8Ga,[19] $RbAu_3In_2$,[8] $NaAu_4Ga_2$,[20] $SrAu_3Ge$,[21] and the

Special Issue: To Honor the Memory of Prof. John D. Corbett

Received: September 30, 2014
Published: December 10, 2014

   dx.doi.org/10.1021/ic502402y | Inorg. Chem. 2015, 54, 1010−1018

Table 1. Details of the Crystal Structure Investigation and Refinement for $BaAu_{5.0}Ga_{2.0}$, $BaAu_{4.3}Ga_{2.7}$, $Ba_{1.04}Au_{4.5}Ga_{2.4}$, $EuAu_{4.8}Ga_{2.2}$, and $Eu_{1.1}Au_{4.4}Ga_{2.2}$

	$BaAu_{5.0}Ga_{2.0}$ (I)	$BaAu_{4.3}Ga_{2.7}$ (II)	$Ba_{1.04}Au_{4.5}Ga_{2.4}$ (III)	$EuAu_{4.8}Ga_{2.2}$ (IV)	$Eu_{1.1}Au_{4.4}Ga_{2.2}$ (V)
fw	1266.86	1171.69	1195.96	1251.21	1199.42
space group	*Pnma*	$P\bar{6}2m$	$P\bar{6}2m$	$P\bar{6}2m$	$P\bar{6}2m$
a, Å	8.855(2)	8.7758(4)	8.7892(4)	8.592(2)	8.5430(8)
b, Å	7.188(1)	8.7758(4)	8.7892(4)	8.592(2)	8.5430(8)
c, Å	20.374(4)	7.1905(8)	7.2124(3)	7.208(2)	7.2493(8)
V, Å^3	1296.9(4)	479.6(1)	482.5(1)	460.8(2)	458.2(1)
Z	8	3	3	3	3
density (calcd), g/cm^3	12.977	12.171	12.348	13.527	13.041
μ, mm^{-1}	127.432	115.238	118.25	133.607	127.03
F(000)	4120	1437	1464	1532	1470
θ range, deg	2.00–28.58°	2.68–32.08°	2.68–28.45°	2.74–25.52°	2.75–30.58
index ranges	$-10 \le h \le 11$	$-13 \le h \le 12$	$-11 \le h \le 11$	$-10 \le h \le 10$	$-11 \le h \le 10$
	$-9 \le k \le 9$	$-12 \le k \le 10$	$-11 \le k \le 11$	$-9 \le k \le 10$	$-11 \le k \le 12$
	$-26 \le l \le 13$	$-10 \le l \le 10$	$-9 \le l \le 9$	$-8 \le l \le 8$	$-10 \le l \le 10$
reflns collected	7838	6617	4273	4983	6307
indep reflns	1677	638	444	358	560
refinement method	full-matrix least squares on F^2				
data/restraints/param	1677/0/87	638/0/31	477/0/38	358/0/31	560/0/32
GOF on F^2	1.00	1.07	1.12	1.07	1.05
final *R* indices [$I > 2\sigma(I)$]	R1 = 0.045, wR2 = 0.093	R1 = 0.031, wR2 = 0.056	R1 = 0.029, wR2 = 0.062	R1 = 0.032, wR2 = 0.057	R1 = 0.034, wR2 = 0.073
R indices (all data)	R1 = 0.071, wR2 = 0.107	R1 = 0.041, wR2 = 0.059	R1 = 0.031, wR2 = 0.063	R1 = 0.041, wR2 = 0.060	R1 = 0.044, wR2 = 0.078
R_{int}	0.078	0.040	0.070	0.090	0.107
largest diff peak and hole, e$^-$/Å^3	3.88 (1.04 Å to Au6) and −4.49 (0.84 Å to Au2)	1.87 (1.35 Å to Au3) and −2.94 (0.69 Å to Au5)	1.76 (1.1 Å to Au6) and −2.82 (1.5 Å to Ba2)	2.13 (0.43 Å to Eu2) and −2.14 (1.02 Å to Au1)	3.23 (0.88 Å to Eu1) and −3.46 (0.72 Å to Au1)

isostructural series $Ae_2Au_6(Au,T)_3$ (Ae = Sr or Ba; T = Zn, Cd, Ga, In, or Sn) and $Sr(Au,Al)_7$.[22−24] On the other hand, the active metal content may also significantly influence the formation of polyanionic networks. For example, studies on Na (K)−Au−Ga and preliminary results with heavier alkali metals show that Na and K do not form compounds with a "cation"/"anion" ratio below 1:7,[3,20] whereas heavier "cations" allow smaller ratios, as low as 1:14, and are well separated by polyanionic frameworks.[25] No Sr/Ba−Au−Ga compounds have been reported until $Ba_2Au_6(Au,Ga)_3$[22] appeared within a family of isostructural compounds.

Following our systematic studies on A−Au−Ga isothermal sections (A = Na, K, Rb, Cs), this work begins the systematic investigation of the Ae−Au−Ga systems (Ae = Ca, Sr, Ba). Our first attempts to produce isostructural Ca−Au−Ga compositions resulted in a completely different chemistry than that for Ba, and these will be described in a subsequent publication.[26] Initial loadings in the Ba−Au−Ga system uncovered the possibility of $NaZn_{13}$-type compounds[27] and led to phases that exhibit hexagonal diamondlike frameworks of Au atoms with voids filled by either Ba or $(Au/Ga)_3$ triangles. In this contribution, the synthesis, structural analysis, electronic structure calculations, and bonding analysis will be presented and discussed.

EXPERIMENTAL SECTION

Synthesis. Starting materials included Ba pieces (99.98%, Alfa Aesar), Eu filings (99.99%, Ames Laboratory), Au particles (99.999%, BASF), and Ga ingots (99.999%, Alfa Aesar). The Eu filings were produced from large ingots, which were mechanically polished prior to use. Mixtures of 300−400 mg total were weighed in N_2- or Ar-filled gloveboxes (H_2O < 0.1 ppmv), loaded into 9 mm Ta ampules, sealed by arc welding under Ar, and then enclosed in evacuated silica jackets or silica Schlenk flasks. The samples were prepared using the following temperature programs: for all Ba-containing samples (**I**–**III**), either heated at 900 °C for 2 h, cooled to 500 °C at a rate of 10 °C/h, then annealed there for 7 days, and cooled by switching off the furnace or heated at 1000 °C for 3 h and quenched into water without further annealing; for Eu-containing structure **IV**, heated to 800 °C in 4 h, kept at this temperature for 14 h, and quenched into water; for **V**, heated to 800 °C in 4 h, kept at this temperature for 12 h, slowly cooled to 300 °C at a rate of 2 °C/h, and quenched into water. Single crystals, which were obtained from samples loaded as "$BaAu_2Ga_2$", "$BaAu_4Ga_2$", "$BaAu_4Ga_3$", "$BaAu_5Ga_2$", "$BaAu_6Ga$", "$BaAu_8Ga_4$", "$Eu_2Au_6Ga_3$", "$Eu_2Au_5Ga_4$", and "$Eu_1Au_4Ga_3$", allowed the possible homogeneity ranges to be analyzed given the number of mixed Ba (Eu)/Au/Ga sites observed in these structures (see Table S3 in the Supporting Information, SI). The compounds exhibit rather narrow solid solutions according to the formulas $BaAu_{5.0}Ga_{2.0(1)}$ (**I**), $BaAu_{4.3}Ga_{2.7(1)}$ (**II**), $Ba_{1.04(2)}Au_{4.5(1)}Ga_{2.4(1)}$ (**III**), $EuAu_{4.8}Ga_{2.2(1)}$ (**IV**), and $Eu_{1.11(1)}Au_{4.4(1)}Ga_{2.2(1)}$ (**V**) obtained from single-crystal X-ray diffraction data. All compounds have metallic luster and are stable against exposure to air or water at room temperature, results that are in accordance with the behavior in related phases.[28]

X-ray Diffraction Studies. Powder X-ray diffraction data were collected at room temperature using a STOE STADI P powder diffractometer equipped with an area detector and Cu Kα_1 radiation (λ = 1.54059 Å). The samples were dispersed on Mylar sheets with the help of vacuum grease and fixed in place with split Al rings. Phase analyses were performed using the *WinXPow 3.0* program. Powder diffraction analyses revealed the title compounds as high-yield products (>90 mol %) in equilibrium with Au_2Ga or a $NaZn_{13}$-type phase with an approximate composition $BaAu_6Ga_6$ (Figures S1−S4 in the SI). Single crystals were fixed on glass fibers and mounted on a Bruker APEX CCD diffractometer. Intensity data were collected at

dx.doi.org/10.1021/ic502402y | *Inorg. Chem.* 2015, 54, 1010−1018

Table 2. Atomic Coordinates and Equivalent Displacement Parameters for $BaAu_{5.0}Ga_{2.0}$, $BaAu_{4.3}Ga_{2.7}$, $Ba_{1.04}Au_{4.5}Ga_{2.4}$, $EuAu_{4.8}Ga_{2.2}$, and $Eu_{1.1}Au_{4.4}Ga_{2.2}$

atom	position	x	y	z	U_{eq}, Å^2	SOF
			$BaAu_{5.0}Ga_{2.0}$ (**I**)			
Ba1	4c	0.2440(2)	0.25	0.06095(7)	0.0105(3)	1
Ba2	4c	0.2691(2)	0.25	0.81181(7)	0.0093(3)	1
Au1	8d	0.5617(1)	0.0484(1)	0.56868(3)	0.0107(2)	1
Au2	8d	0.0516(1)	0.0473(1)	0.19939(3)	0.0117(2)	1
Au3	8d	0.0994(1)	0.0439(1)	0.44279(3)	0.0121(2)	1
Au4	8d	0.1185(1)	0.0527(1)	0.67390(3)	0.0130(2)	1
Au5/Ga5	4c	0.3264(1)	$^1/_4$	0.51135(5)	0.0108(3)	0.956/0.044(7)
Au6/Ga6	4c	0.0778(2)	$^1/_4$	0.32162(6)	0.0134(4)	0.677/0.323(7)
Au7/Ga7	4c	0.3048(3)	$^1/_4$	0.2475(1)	0.0184(7)	0.308/0.692(7)
Ga8	4c	0.0580(4)	$^1/_4$	0.5629(1)	0.0100(6)	1
Ga9	4c	0.3346(3)	$^1/_4$	0.3778(1)	0.0093(6)	1
Ga10	4c	0.3631(3)	$^1/_4$	0.6406(1)	0.0089(6)	1
			$BaAu_{4.3}Ga_{2.7}$ (**II**)			
Ba1	1a	0	0	0	0.0098(7)	1
Ba2	2d	$^1/_3$	$^2/_3$	$^1/_2$	0.0102(5)	1
Au1	6i	0.6986(1)	0	0.2997(1)	0.0145(3)	1
Au2/Ga2	6i	0.3684(1)	0	0.2074(1)	0.0119(3)	0.77/0.23(1)
Au3/Ga3	6j	0.2915(3)	0.4795(3)	0	0.0173(6)	0.268/0.732(6)
Au4/Ga4	3g	0.1932(3)	0	$^1/_2$	0.0127(8)	0.216/0.784(9)
			$Ba_{1.0}Au_{4.5}Ga_{2.4}$ (**III**)			
Ba1	1a	0	0	0	0.0127(7)	1
Ba2	2d	$^1/_3$	$^2/_3$	$^1/_2$	0.0129(7)	0.93(1)
Au0/Ga0	6k	0.478(3)	0.633(3)	$^1/_2$	0.0129(7)	0.03/0.04(1)
Au1	6i	0.7013(1)	0	0.2986(1)	0.0182(3)	1
Au2/Ga2	6i	0.3625(1)	0	0.2052(1)	0.0180(3)	0.95/0.05(1)
Au3/Ga3	6j	0.3146(3)	0.4923(4)	0	0.0250(7)	0.21/0.66(1)
Ba3	2c	$^1/_3$	$^2/_3$	0	0.012(5)	0.13(1)
Au4/Ga4	3g	0.1904(4)	0	$^1/_2$	0.0220(11)	0.13/0.87(1)
			$EuAu_{4.8}Ga_{2.2}$ (**IV**)			
Eu1	1a	0	0	0	0.0118(15)	1
Eu2	2d	$^1/_3$	$^2/_3$	$^1/_2$	0.0140(12)	1
Au1	6i	0.6966(2)	0	0.3030(2)	0.0154(5)	1
Au2	6i	0.3699(3)	0	0.2109(3)	0.0209(6)	1
Ga3/Au3	6j	0.2891(6)	0.4755(6)	0	0.0214(14)	0.71/0.29(1)
Ga4/Au4	3g	0.1977(8)	0	$^1/_2$	0.020(2)	0.78/0.22(2)
			$Eu_{1.1}Au_{4.4}Ga_{2.2}$ (**V**)			
Eu1	1a	0	0	0	0.0083(9)	1
Eu2	2d	$^1/_3$	$^2/_3$	$^1/_2$	0.0117(7)	1
Au1	6i	0.7002(2)	0	0.3014(2)	0.0105(3)	1
Au2	6i	0.3674(2)	0	0.2079(2)	0.0122(3)	1
Ga3/Au3	6j	0.3033(6)	0.4816(7)	0	0.0188(11)	0.64/0.19(1)
Eu3	2c	$^1/_3$	$^2/_3$	0	0.0188(11)	0.17(1)
Ga4/Au4	3g	0.2004(7)	0	$^1/_2$	0.0098(15)	0.93/0.07(1)

~293 K with Mo Kα radiation (λ = 0.71073 Å) in φ- and ω-scan modes using at least 1600 frames and exposures of 15−20 s/frame. The reflection intensities were integrated using the *SAINT* program in the *SMART* software package[29] over the entire reciprocal sphere. Empirical absorption corrections were accomplished with the aid of the *SADABS* program.[30]

The initial atomic parameters were obtained via direct methods (*SHELXS-97*).[31] Space groups were determined by *XPREP* algorithms as coded in the *SHELXTL* program package.[32] Structure refinement succeeded in space groups *Pnma* (No. 62) for **I** and $P\bar{6}2m$ (No. 189) for **II**−**V**. Full matrix least-squares refinements on F^2 with anisotropic atomic displacement parameters were employed for all atoms using the *WinGX* program package.[33] **III**−**V** were refined as racemic twins. On the basis of the absolute structure parameter, the assignment of the absolute structure of **II** was verified. Analyses of the difference Fourier maps for the initial "$AeAu_{4+x}Ga_{3-x}$" models in the hexagonal structures of **III** and **V** (see Figure S6 in the SI) and the respective solid solutions revealed large electron density peaks located at the centers of the Au3/Ga3 (Wyckoff site 2c) and Au4/Ga4 (Wyckoff site 1b) triangles. However, additional examination of the diffraction data for these structures did not provide any likely hints for the presence of merohedral twinning. Closer inspection of the proximities for these peaks and the thermal parameters for the mixed (Au, Ga) sites pointed to the presence of mixed Ae/$(Au,Ga)_3$ occupancies. Refinements using mixed Ae3/(Au3/Ga3) and Ae4/(Au4/Ga4) occupancies (see Table 2 and CIF files in the SI) proceeded to significantly smaller residual peaks. For instance, the largest peaks in the difference Fourier map of hexagonal $Eu_{1.1}Au_{4.4}Ga_{2.2}$ (**V**) were 3.23 e$^-$/Å^3 (0.88 Å to Eu1) and −3.46 e$^-$/Å^3 (0.72 Å to Au1; see Table 1). Details of the data collection and refinement parameters for four prototypical crystals are

dx.doi.org/10.1021/ic502402y | *Inorg. Chem.* 2015, 54, 1010−1018

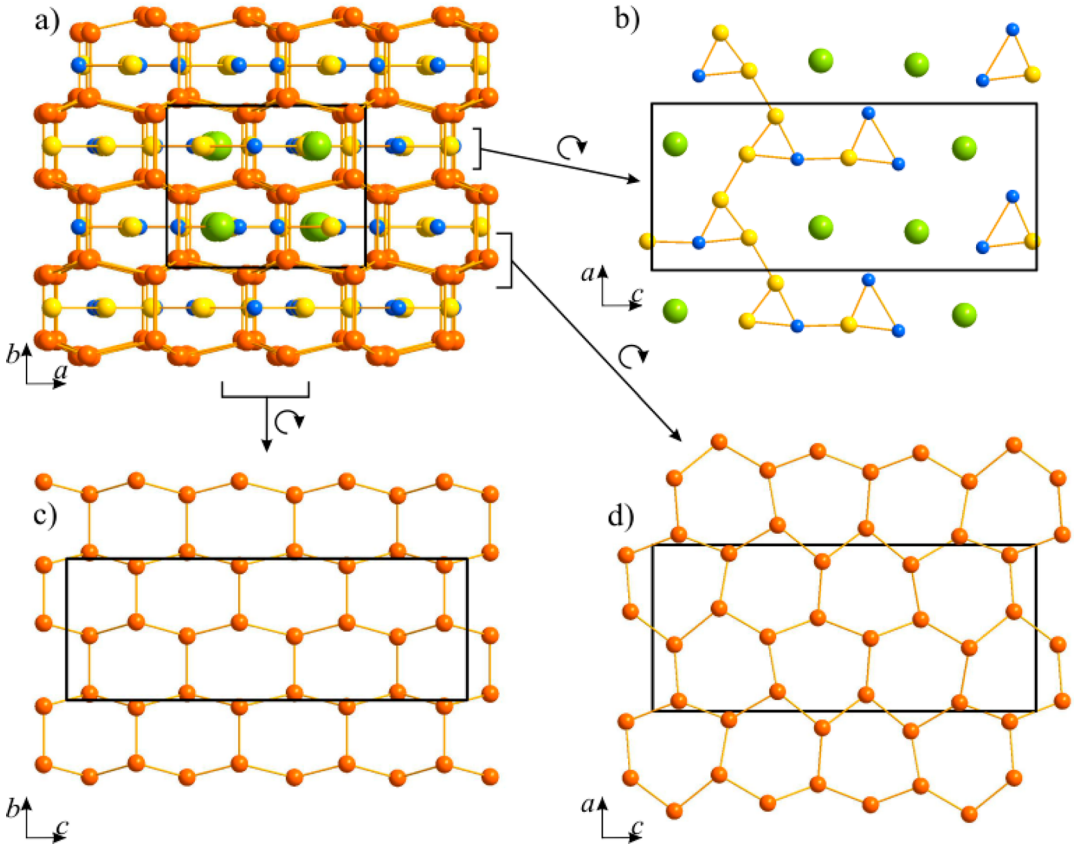

Figure 1. Crystal structure of **I**: (a) projection along the long *a* axis; (b) layers containing interstitial M_3 groups and Ba atoms; Au layers formed from hexagons in (c) boat and (d) chair conformations. Au atoms are orange, Ga blue, Au/Ga yellow, and Ba green.

provided in Table 1, and their atomic positions are listed in Table 2. All remaining crystallographic information can be found in the SI as CIF files.

Electronic Structure Calculations. Calculations were performed on hypothetical models constructed by representing all mixed Au/Ga positions by the corresponding majority occupant, resulting in the compositions "$BaAu_5Ga_2$" for **I** and "$BaAu_4Ga_3$" for **II**. As starting points for the electronic structure calculations, coordinates obtained from structure optimizations using the *VASP* code were used. Details can be found in the SI. The calculations utilized the self-consistent, tight-binding (TB), linear-muffin-tin-orbital (LMTO) method in the local density and atomic sphere (ASA) approximations, using the Stuttgart code.[34] The radii of the Wigner–Seitz spheres were assigned automatically so that the overlapping potentials would be the best possible approximations to the full potentials. They were 2.33 and 2.37 Å for Ba1 and Ba2, 1.52, 1.51, 1.50, 1.62, 1.62, and 1.51 Å for Au1–Au6, and 1.44, 1.43, 1.45, and 1.45 Å for Ga7–Ga10 in "$BaAu_5Ga_2$" and 2.34 and 2.32 Å for Ba1 and Ba2, 1.62 and 1.54 Å for Au1 and Au2, and 1.50 and 1.48 Å for Ga1 and Ga2 in "$BaAu_4Ga_3$". No interstitial spheres were needed to achieve space filling in either case. The basis sets were 5d/4f/6s/(6p) for Ba, 5d/(5f)/6s/6p for Au, and 4s/4p/(4d) for Ga, with orbitals in parentheses downfolded.[35] Scalar relativistic effects were included in the calculations. The band structures were sampled for 155 and 125 *k* points in the corresponding irreducible wedges of the Brillouin zones for "$BaAu_5Ga_2$" and "$BaAu_4Ga_3$", respectively. To perform bonding analyses, crystal orbital Hamilton populations (COHPs) for selected atom pairs, as well as their weighted sums over all filled electronic states, ICOHP,[36] were evaluated.

RESULTS AND DISCUSSION

Initial explorations of the Ba-poor (<15 atom %) part of the Ba–Au–Ga system have resulted in the discovery of three Au-rich phases, $BaAu_{5.0}Ga_{2.0}$ (**I**), $BaAu_{4.3}Ga_{2.7}$ (**II**), and $Ba_{1.04}Au_{4.5}Ga_{2.4}$ (**III**). No systematic studies have been reported for this system since the first detection of a solid solution based on $BaGa_4$;[37] however, the recent discovery of $Ba_2Au_6(Au,T)_3$,[22] in which T represents a number of post-transition elements including Ga, has sparked our interest. Both compounds are located in a small triangular region bordered by $BaAu$[40]–$BaAu_2$[15]–Au_2Ga.[38]

Crystal Structures. $BaAu_5Ga_2$ (**I**) crystallizes with an orthorhombic unit cell in its own structure type, which involves three interpenetrating, mutually orthogonal hexagonal Au networks that form stacks of puckered honeycombs (Figure 1a). Various projections of the Au framework are presented in Figure 1. The hexagons in two orthogonal planes along the *b* axis adopt boat conformations, whereas those in the *ac* plane adopt the chair arrangement to form a hexagonal diamond net, as found for In atoms in $CaIn_2$.[39] The resulting voids of this net can accommodate Ba atoms or triangular clusters of Au and Ga atoms (M_3; Figures 1a,b). As such, the structure is related to AlB_2-type $BaAu_2$.[15] Because each Au atom of the framework belongs to 6 such voids and each Ba atom or M_3 group is surrounded by 12 Au atoms, the general composition of these phases takes the form $(Au_{12/6}Ba)_m(Au_{12/6}M_3)_n$. From Figure 1b, there are equal numbers of Ba and M_3 groups in the structure of **I**, 8 per unit cell, and each M_3 triangle is $\sim(AuGa_2)$ to yield the formulation $(Au_{12/6}Ba)_8(Au_{12/6}M_3)_8 \cong Ba_8Au_{32}(M_3)_8 \approx Ba_8Au_{32}(AuGa_2)_8 \cong BaAu_4(AuGa_2) = BaAu_5Ga_2$.

There are two different kinds of Au positions (see Figure 1): (1) Au1–Au4 (orange) atoms build the hexagonal diamond-

dx.doi.org/10.1021/ic502402y | Inorg. Chem. 2015, 54, 1010–1018

type net; (2) positions M5−M7 (yellow), which are mixed occupied by 31−96% Au and with the Ga8−Ga10 sites, form 1D ribbons along the *a* axis consisting of two types of M_3 triangles in the *ac* plane. The M_3 triangles forming the backbone of the ribbon (positions M6, M7, and Ga9) exhibit an average composition of ~$AuGa_2$ ($Au_{0.99}Ga_{2.01(1)}$), but the distribution of Au and Ga atoms on the M6 and M7 positions allows for three different clusters (20.9% Au_2Ga + 56.8% $AuGa_2$ + 22.4% Ga_3) and creates nearly equilateral triangles. The M_3 triangles on the periphery of the ribbons show less variation in composition, i.e., also ~$AuGa_2$ ($Au_{0.96}Ga_{2.04(1)}$ = 95.6% $AuGa_3$ + 4.4% Ga_3), but are more distorted with an unusual Ga−Ga distance (Ga8−Ga10) of 3.13 Å. This value is considerably larger than the sum of the covalent radii[40] and arises from strong Au−Ga contacts that exist within and between the M_3 groups as well as with the Au framework. In spite of their very similar composition, $BaAu_5Ga_2$ and $SrAu_{5+y}Al_{2-y}$ represent two alternative ways to arrange the Ba or Sr atoms and M_3 groups. In $SrAu_{5+y}Al_{2-y}$, all M_3 groups are ~$AuAl_2$ and form simple zigzag chains with all intergroup heteroatomic Au−Al contacts. In $BaAu_5Ga_2$, however, the occupancies of the M6 and M7 positions preclude only heteroatomic Au−Ga bonds between M_3 triangles.

Another question concerns how mutually replaceable the M_3 triangles and Ba cations are. These two species are quite different chemically and geometrically, but, nevertheless, the Au framework can accommodate both in similar environments, although not without local changes. The average size of each M_3 group in the *ac* plane is comparable to Ba, and that along the *b* axis, to Ga (Au). The shape and orientation of the M_3 triangle in the *ac* plane are responsible for a considerable distortion of the Au network in the aristotypic AlB_2-type $BaAu_2$,[15] resulting in the hexagonal diamond network with two kinds of interlayer Au−Au distances: a shorter group (2.9−3.0 Å) separated by M_3 edges and a longer group (4.3−4.4 Å) by M_3 vertices. All M_3 groups alternate with Ba atoms along the *b* axis and are evenly distributed in the *ac* plane, forming identical structural motifs (Figure 1b). The corresponding Ba coordination polyhedra (CN = 24) also form two parallel branched zigzag chains along the *a* axis (Figure S5 in the SI).

$BaAu_{4.3}Ga_{2.7}$ (**II**) and $EuAu_{4.8}Ga_{2.2}$ (**IV**) (Figure 2) are formally isostructural with $SrAu_{4.06}Al_{2.94}$,[24] but several features do not allow these three structures to be strictly identical. All structures are composed of hexagonal diamond frameworks built from two inequivalent Au sites (Au1 and Au2 in **II** and **IV**), with Ae cations and triangular $(Au/Ga)_3$ clusters encapsulated in the prismatic voids. The most noticeable difference is that $SrAu_{4.06}Al_{2.94}$ exhibits almost no mixing of Au and Al atoms, resulting in a nearly stoichiometric composition $SrAu_4Al_3$, whereas there are no fully occupied Ga positions in **II** or **IV** (Table 2). Moreover, Au atoms fully occupy the hexagonal diamond net in $SrAu_{4.06}Al_{2.94}$[24] and in **IV**, whereas Ga atoms in **II** are significantly involved in this substructure (Table 3). So, the structure of **II** involves a formal anion exchange between the 3D network and interstitial M_3 triangles, a feature that had not been observed among any related phases but that also influences the structure of the framework and composition of the M_3 triangles. In contrast to **I**, there are two inequivalent alternating Ba/M_3 layers in **II** (Figure 2b,d), and all M_3 triangles are equilateral but with different M−M distances, i.e., 2.586 or 2.937 Å. Because some Ga atoms belong to the hexagonal diamond network, the total amount of Au in the M_3 triangles is higher (22−27%) compared to 0−13% in $SrAu_{4.06}Al_{2.94}$. Another interesting difference between **I** and **II** is the slight elongation of the interlayer Au−Au distances (within the "boats"). In spite of the partial substitution of Au by Ga, these Au−Au distances in **I** are slightly shorter (2.837−2.964 Å) than those in **II** (2.880−2.982 Å); however, Au−Au distances within the "chair" layers are shorter in **II** (2.973−3.056 Å), showing a significantly smaller distortion of the honeycombs compared to **I**. Compound **IV** resembles **II**, with Au−Au distances ranging from 2.884 to 3.009 Å in the "chairs" and from 2.840 to 3.040 Å between the "chair"-fashioned Au layers.

Finally, the crystal structures of hexagonal **III** and **V** can be derived from those of **II** and **IV**, respectively. Yet, **III** and **V** differ from **II** and **IV** because the triangular $(Au/Ga)_3$ clusters are partially replaced by Ba or Eu (Ae atoms; see Table 3 and Figure S6 in the SI). To the best of our knowledge, such $Ae/(Au/Ga)_3$ admixing has not been observed for any other structure type with a diamond-like Au framework, yet formally partial replacements of cations by anionic subunits have been recently reported for the binaries $Ae_{3-x}Ga_{8+3x}$ [Ae = Sr (x = 0.15), Eu (x = 0.12)].[41,42]

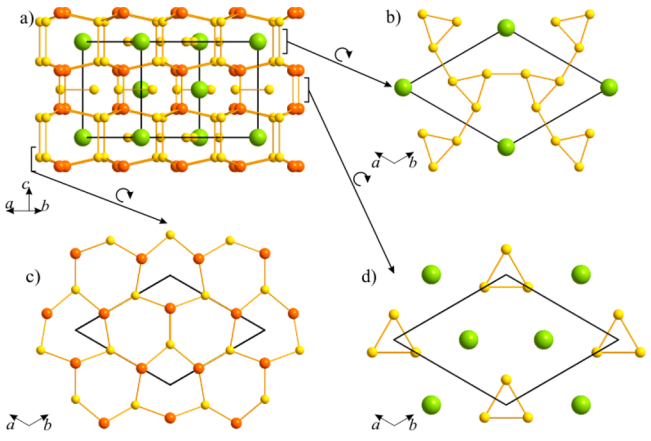

Figure 2. Crystal structure of **II**: (a) projection along [010]; (c) layer containing Au and mixed Au/Ga positions that form hexagonal diamond-like net; (b and d) Au/Ga and Ba interstitial layers. Au atoms are orange, Au/Ga yellow, and Ba green.

Structural Analysis. The five structures identified by this study can all be derived from the binary $BaAu_2$ (AlB_2-type; space group *P6/mmm*)[15] or $EuAu_2$ ($CeCu_2$-type; space group *Imma*)[43] by replacing some of the Ba or Eu atoms with $(Au,Ga)_3$ triangles to achieve the formulations $[Ae_x[(Au,Ga)_3]_{1-x}]Au_2$ (Ae = Ba or Eu), although structures **II** and **III** indicate some Ga atom substitution for Au "majority component" sites, i.e., $[Ba_x[(Au,Ga)_3]_{1-x}](Au,Ga)_2$. $BaAu_2$ is constructed exclusively from condensed $Au_{12/6}Ba$ hexagonal prisms that show short Au−Au distances within the hexagons (2.77 Å) and much longer distances between them (4.12 Å) to create graphene-like 2D planar hexagonal nets of Au atoms.[15] In orthorhombic $EuAu_2$, the corresponding hexagons adopt a chairlike conformation showing a range of Au−Au distances (2.71−2.91 Å) as well as two distinct Au−Au distances (2.92 and 4.41 Å) between hexagons to create a 3D distorted tetrahedral net of Au atoms. Nevertheless, the coordination environment of Eu still consists of 12 Au atoms, so that $EuAu_2$ can also be built of condensed $Au_{12/6}Eu$ polyhedra.

Topological analysis of compounds **I**−**V** suggests that they are components of the sequence $(Au_{12/6}Ae)_m(Au_{12/6}M_3)_n$,

dx.doi.org/10.1021/ic502402y | Inorg. Chem. 2015, 54, 1010−1018

Table 3. Fractional occupations of the Ae2(Au0/Ga0), Ae3(Au3/Ga3), and Ae4(Au4/Ga4) in the hexagonal $BaAu_{4.3}Ga_{2.7}$, $Ba_{1.0}Au_{4.5}Ga_{2.4}$, $EuAu_{4.8}Ga_{2.2}$, and $Eu_{1.1}Au_{4.4}Ga_{2.2}$[a]

compound	Ae2/(Au0/Ga0)	(Au2/Ga2)	Ae3/(Au3/Ga3)	Ae4/(Au4/Ga4)	crystal
$BaAu_{4.3}Ga_{2.7}$	1/(0/0)	(0.77/0.23)	0/(0.27/0.73)	0/(0.22/0.78)	**II**
$Ba_{1.0}Au_{4.5}Ga_{2.4}$	0.93/(0.03/0.04)	(0.95/0.05)	0.13/(0.21/0.66)	0/(0.13/0.87)	**III**
$EuAu_{4.8}Ga_{2.2}$	1/(0/0)	(1/0)	0/(0.71/0.29)	0/(0.78/0.22)	**IV**
$Eu_{1.1}Au_{4.4}Ga_{2.2}$	1/(0/0)	(1/0)	0.17/(0.64/0.19)	0/(0.93/0.07)	**V**
$Eu_{1.1}Au_{4.4}Ga_{2.2}$	1/(0/0)	(1/0)	0.16/(0.15/0.69)	0.08/(0.14/0.78)	**S1**

[a]Parentheses represent sites that possess mixed Au/Ga occupation in blue. Additionally, $Eu_{1.1}Au_{4.4}Ga_{2.2}$ (crystal S1) shows Eu admixing on the Au4/Ga4 site.

where m and n are the neighboring members of the Fibonacci row: $m = 1$, $n = 0$ results in $AeAu_2$, $m = 1$, $n = 1$ in $AeAu_4M_3$ [$SrAu_{4.06}Al_{2.94}$,[24] $EuAu_{4.8}Ga_{2.2}$ (**IV**), $BaAu_5Ga_2$ (**I**), and $BaAu_{4.3}Ga_{2.7}$ (**II**)], and finally $m = 2$, $n = 1$ in $Ba_2Au_6M_3$ ($Sr_2Au_{6.18}Al_{2.82}$[24] and $Ba_2Au_7Ga_2$[22]). A representative with $m = 3$ and $n = 2$ was never observed; however, more detailed investigations of this composition led to the discovery of $Ba_{1.04}Au_{4.5}Ga_{2.4}$ (**III**) and $Eu_{1.1}Au_{4.4}Ga_{2.2}$ (**V**), both of which provide a very important clue that can account for this fact. At first glance, structures **III** and **V** are very close to the general composition "AeM_7" and contain identical units filling the cavities of the hexagonal diamond network, yet the manner of filling is unprecedented in other ternary cases. Compounds **III** and **V** are the first examples of this class of polar intermetallic structures in which formally anionic M_3 groups can be partially replaced by formally cationic Ae atoms with essentially no or, at most, very minor changes to their corresponding coordination environments. Such mixing might be possible because of the major participation of Ae valence orbitals in covalent bonding. Perhaps the closest analogues come from polar intermetallics containing lithium, which, because of its higher electronegativity and small size, is frequently involved in anionic substructures of polar intermetallics.[44,45] This specific analogy, however, is distinctly opposite from structures **III** and **V** and offers no examples of cation−anion exchange. In the In−Sb−Zn system, structures feature a *statistical* distribution of transition-metal (Zn) and late-main-group metal (In) distributions over one site while maintaining an Sb host lattice.[46] However, in $Zn_5Sb_4In_{2-\delta}$ ($\delta = 0.15$) and $Zn_9Sb_6In_2$, square-antiprismatic cages of Sb are connected through additional all-faces-capped tetrahedra and do not allow any direct comparison to the **I**−**V** phases, in which cationic Ae atoms and anionic M_3 groups are *nonstatistically* distributed. To understand the composition/structure relationships in these compounds in more detail, we follow up with an analysis of the electronic structures for the Ba-containing compounds **I** and **II**.

Electronic Structure and Bonding Analysis. Electronic structure calculations have been performed for slightly modified models of **I** and **II** because of challenges to treat partially occupied sites in the asymmetric units. For compound **I**, the idealized composition of "$BaAu_5Ga_2$" was achieved by assigning Au atoms to sites M5 and M6 and Ga atoms to site M7; for compound **II**, the model "$BaAu_4Ga_3$" was constructed by placing Au atoms at the M2 sites and Ga atoms at the M3 and M4 sites. The resulting compositions are reasonably good approximations to the observed ones. Total energy calculations using *VASP* on models of identical composition but different site occupancies of Au and Ga revealed that these stated models for **I** ("$BaAu_5Ga_2$") and **II** ("$BaAu_4Ga_3$") are, indeed, the lowest-energy structures (see the SI).

The electronic densities of states (DOSs) curves for "$BaAu_5Ga_2$" and "$BaAu_4Ga_3$" are presented in Figures 3a and

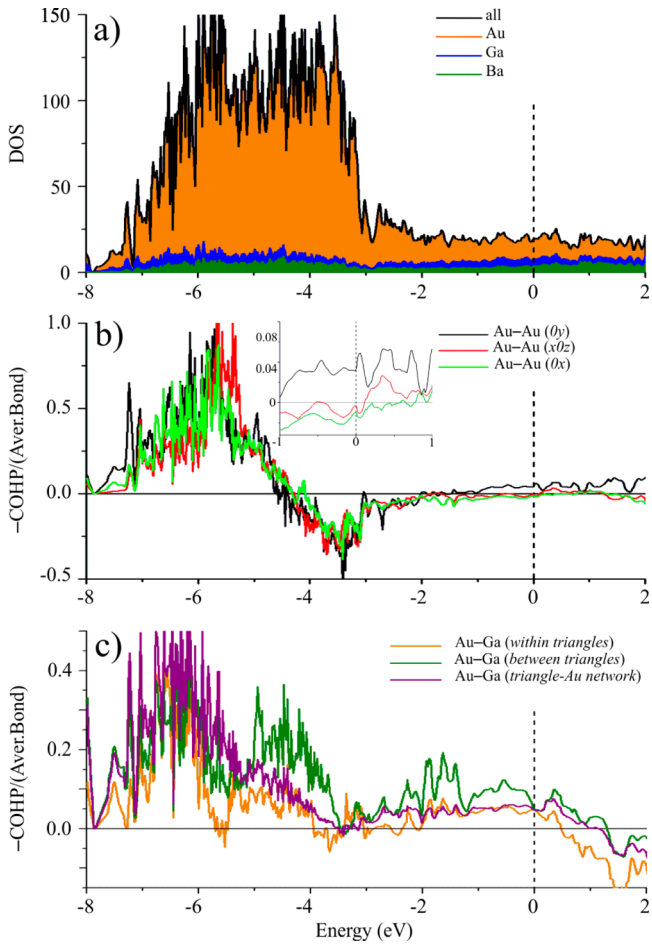

Figure 3. Results of LMTO-ASA calculations for "$BaAu_5Ga_2$" (E_F is the dotted black line). DOSs: total DOS (black) and partial DOS curves for Au (orange), Ga (blue), and Ba (green) (a). −COHP data for Au−Au interactions: vertical (boats, black), horizontal (chairs, green and common, red) (b). −COHP data for Au−Ga interactions: within triangles (orange), between triangles (green), and between triangles and the Au framework (violet) (c).

4a. Both exhibit broad valence bands extending ∼12 eV below the Fermi level (E_F) and including large, mostly Au 5d, bands found 3−7 eV below E_F. This 5d band is distinctly broader in the DOS of "$BaAu_5Ga_2$" and resembles the corresponding 5d bands in the DOS curves evaluated for the Au-rich phases $Ba_2Au_7Ga_2$[22] and $NaAu_4Ga_2$.[20] The DOS regions near the corresponding Fermi levels are relatively flat and nonzero to suggest that both compounds should be metallic. For

dx.doi.org/10.1021/ic502402y | Inorg. Chem. 2015, 54, 1010−1018

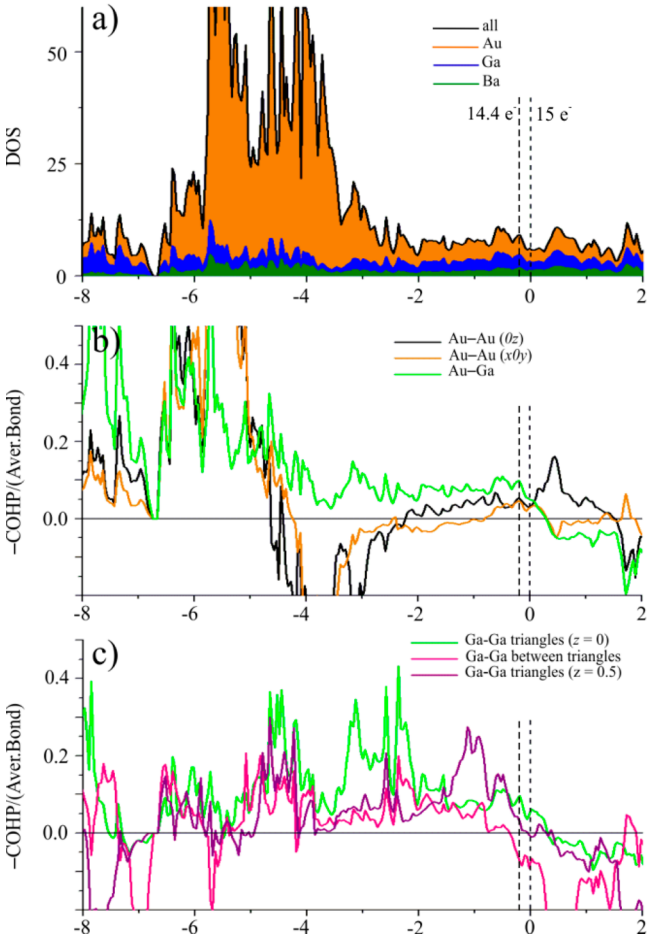

Figure 4. Results of LMTO-ASA calculations for "$BaAu_4Ga_3$" (E_F is the dotted black line). DOSs: total DOS (black) and partial DOS curves for Au (orange), Ga (blue), and Ba (green) (a). −COHP data for Au−Au and Au−Ga interactions: Au−Au vertical (black), Au−Au horizontal (orange,) and Au−Ga (violet) (b).−COHP data for Ga−Ga interactions: within triangles at z = 0 (green), within triangles at z = 0.5 (violet), and between triangles at z = 0 (rose) (c).

"$BaAu_4Ga_3$", a ∼0.5 eV wide pseudogap can be discerned around the calculated E_F. Because compound **II** refines as $BaAu_{4.3}Ga_{2.7}$, which has 14.4 valence electrons per formula unit, the Fermi level will occur near the lower part of the pseudogap, as indicated in Figure 4a. For "$BaAu_5Ga_2$", however, a similar pseudogap in the DOS occurs at ∼0.65 eV above the Fermi level, which corresponds to 14.7 valence electrons per formula unit, whereas the refined composition has 13 valence electrons. Thus, the theoretically "optimal" value is only achievable by almost complete replacement of one Au atom by Ga. However, this occurrence was not observed during explorations, which revealed a very limited homogeneity range for **I**. Another possibility to increase the valence electron count can transpire by replacing Ga with Sn; such a substitution has been observed in the series of isostructural compounds $Ba_2Au_6(Au,T)_3$.[22] However, this result may also suggest a lower importance of the valence electron concentration toward influencing these structure types.

Analysis of the partial DOS curves reveals comparable contributions from Ba (6s and 5d) and Ga (4s and 4p) valence orbitals but major contributions from valence 6s, 6p, and 5d orbitals of Au over the entire occupied range. The contributions from Ba to the DOS differentiate it from the active metals K, Rb, or Cs[3] and suggest that Ba does not donate all of its valence electrons to the Au−Ga substructure. It is also remarkable that Ba orbital contributions are somewhat higher than those of Ga in spite of the doubled Ga content in the compound.

To compare interatomic interactions, COHP analyses were carried out (see Figures 3b,c and 4b,c). The ICOHP results for selected contacts are summarized in Table S2 in the SI. The most interesting question in "$BaAu_5Ga_2$" (**I**) is the significance of orbital interactions within the hexagonal diamond-like Au framework, not at least because there are significantly more homoatomic Au−Au contacts in the formally anionic network than heteroatomic Au−Ga or Ba−Au bonds. It should be mentioned that the major proportion of Au in the formula unit does not always mean predominance of the homoatomic Au−Au contacts. For example, another Au-rich compound, $NaAu_4Ga_2$,[20] contains nearly twice as many Au−Ga contacts as Au−Au contacts, showing the large influence of symmetry and local atomic arrangements. As seen from Figure 3b, there are significant differences among Au−Au orbital interactions along different directions in the structure of "$BaAu_5Ga_2$". All bonds along the b direction (in the boat conformations), which are also the shortest Au−Au contacts, remain bonding at and above the Fermi level and have the largest ICOHP values, 0.96−1.16 eV/(average bond). The Au−Au bonds in the ac plane (in the chair conformations), which were formally divided into two groups along different directions, are qualitatively similar, show smaller ICOHP values [0.63−0.93 eV/(average bond)], and are slightly antibonding at E_F. Such orbital interactions are, in fact, opposite to the case of graphite, with strong intralayer and very weak interlayer interactions. No major differences were detected for Au−Ga interactions in the three formally different groups: within M_3 units and between M_3 and the Au framework (Figure 3c). Adding valence electrons would shift all Au−Au interactions into the bonding region while simultaneously decreasing the Au−Ga and Au−Au ($\|b$) interactions. A cardinally different situation was observed for "$BaAu_4Ga_3$". With ∼30% higher Ga content than "$BaAu_5Ga_2$", the number of heteroatomic Au−Ga contacts increases considerably and is now larger than the number of homoatomic Au−Au bonds. Such Ga doping affected all interactions in the structure qualitatively and quantitatively. In spite of somewhat different Au−Au distances within the boat and chair conformations, ICOHP values in all directions show nearly identical distributions (Table S2 in the SI) and maintain bonding at and slightly above the Fermi level (Figure 4b).

Au−Ga interactions in both compounds are qualitatively comparable with Au−Au interactions in "$BaAu_4Ga_3$" or Au−Au contacts along the b axis in "$BaAu_5Ga_2$" near the Fermi level; however, their ICOHP values are significantly higher (Table S2 in the SI). The last is rather typical for all A−Au−Ga compounds, e.g., as calculated for various examples in the K−Au−Ga system.[3] It is not unexpected that Au−Au and Au−Ga contacts provide the greatest contributions to the total orbital interactions, but the ICOHP values of 0.30−0.45 eV/bond evaluated for Ba−Au contacts could not be expected for the heavier alkali metal−Au interactions. Ba−Au and Ba−Ga contacts show ICOHP values comparable to those of Au−Ga at the Fermi level (Figure S8 in the SI). Furthermore, the only "pure" Ga−Ga contact in the structure of **I** (3.134 Å) cannot be characterized as a bonding interaction, whereas short M7−Ga9 contacts involving a minor contribution from Au atoms show a fairly high ICOHP value. On the other hand, the limited number of these contacts cannot play a major role in the

dx.doi.org/10.1021/ic502402y | Inorg. Chem. 2015, 54, 1010−1018

general picture. All Ga sites form triangles with short contacts and strong interactions with neighboring Au atoms. Two M_3 (Ga_3 as included in the calculation) triangles in "$BaAu_4Ga_3$" (at $z = 0$ and $^1/_2$) also exhibit different bonding situations (Figure 4c). Ga−Ga interactions at $z = 0$ (2.586 Å) are strong and bonding at E_F, whereas those at $z = 0.5$ (2.937 Å) are rather nonbonding. In this case, removing valence electrons according to the refined composition $BaAu_{4.3}Ga_{2.7}$ would move these interactions into the bonding region. The third type of Ga−Ga contacts, that between the triangles at $z = 0$, are strongly antibonding at the Fermi level. However, all Ga positions have significant connections to the Au atoms forming the hexagonal diamond framework. This feature might explain the minor importance of geometrical factors over the wide variability of the transition metals forming the related $Ba_2Au_6(Au,T)_3$ type and existence of Au/T solid solutions with some post-transition elements.[22]

Physical Properties. Magnetic susceptibility data were collected for "$BaAu_5Ga_2$" in a temperature range from 2 to 300 K on a Quantum Design (MPMS) SQUID magnetometer. A polycrystalline sample of 30.7 mg total weight was loaded in a fused-silica capillary and measured at a constant field of 1 kOe (see Figure S9 in the SI). The small, positive, almost temperature-independent susceptibility of **I** ($\chi_m \approx 8.1 \times 10^{-5}$ emu/mol) suggests this compound to be a Pauli paramagnet, which is in full conformity with the results of the band structure calculations.

CONCLUSIONS

The Ae-poor parts of the Ba−Au−Ga and Eu−Au−Ga systems have been investigated, leading to the discovery of five Au-rich compounds. $BaAu_5Ga_2$ (**I**) crystallizes in its own structure type and exhibits complex 3D hexagonal diamond-like Au network. $BaAu_{4.3}Ga_{2.7}$ (**II**) and $Ba_{1.04}Au_{4.5}Ga_{2.4}$ (**III**) represent unprecedented examples with a post-transition element partially involved in the formation of the hexagonal diamond-like Au framework; however, the Eu-containing analogue, i.e., $EuAu_{4.8}Ga_{2.2}$ (**IV**), does not exhibit any Ga mixing into the Au network. In contrast to the prototypical $SrAu_{4.06}Al_{2.94}$,[24] all hexagonal structures show significant mixing of Au and Ga in the triangular M_3 clusters. The homologous series based on the binary compounds $AeAu_2$ and the general formulation $(Au_{12/6}Ae)_m(Au_{12/6}M_3)_n$ have been uncovered, with the present compounds being its third members. Compounds **III** ($Ba_{1.0}Au_{4.5}Ga_{2.4}$) and **V** ($Eu_{1.1}Au_{4.4}Ga_{2.2}$) represent the very rare cases of mutual exchange between cations and anions or anionic groups.

Analysis of TB-LMTO-ASA calculations for "$BaAu_5Ga_2$" and "$BaAu_4Ga_3$" shows that all compounds should be metallic, and the overall bond populations are dominated by homoatomic Au−Au and polar Au−Ga bonds. The contributions from these two pairs in $BaAu_5Ga_2$ into the total bonding interactions are comparable, an outcome that is unusual for Au-rich polar intermetallics.[3] COHP analysis also revealed anisotropic distributions of Au−Au interactions that are opposite to those observed in graphite-type structures. "$BaAu_4Ga_3$" shows more isotropic distributions of Au−Au and Au−Ga interactions approaching those in the diamond structure. Ga−Ga bonding interactions in both cases are strongly affected by the Au network, and Ba atoms, in spite of their low electronegativity, were found to be significantly involved in polar-covalent Ba−Au and Ba−Ga interactions as well.

ASSOCIATED CONTENT

Supporting Information

Tables of the anisotropic displacement parameters for compounds **I**−**V**, ICOHP values for selected bonds in the structures of **I** and **II**, observed and calculated powder X-ray diffraction patterns for compounds **I**−**V**, magnetic data for compound **I**, and crystallographic information in CIF format. This material is available free of charge via the Internet at http://pubs.acs.org.

AUTHOR INFORMATION

Corresponding Authors

*E-mail: mudring@iastate.edu.
*E-mail: gmiller@iastate.edu.

Notes

The authors declare no competing financial interest.

ACKNOWLEDGMENTS

The research was supported in part by the Critical Materials Institute, an Energy Innovation Hub, funded by the U.S. Department of Energy (DOE), Office of Energy Efficiency and Renewable Energy, Advanced Manufacturing Office, and the Office of the Basic Energy Sciences, Materials Sciences Division, DOE, and the Department of Materials Science and Engineering at Iowa State University. Ames Laboratory is operated for DOE by Iowa State University under Contract DE-AC02-07CH11358.

DEDICATION

Dedicated to the memory of Prof. John D. Corbett.

REFERENCES

(1) Corbett, J. D. *Inorg. Chem.* **2010**, *49*, 13−28.
(2) Pyykkö, P. *Angew. Chem., Int. Ed* **2004**, *43*, 4412−4456.
(3) Smetana, V.; Corbett, J. D.; Miller, G. J. *Inorg. Chem.* **2012**, *51*, 1695−1702.
(4) Smetana, V.; Miller, G. J.; Corbett, J. D. *Inorg. Chem.* **2012**, *51*, 7711−7721.
(5) Lin, Q.; Smetana, V.; Miller, G. J.; Corbett, J. D. *Inorg. Chem.* **2012**, *51*, 8882−8889.
(6) Smetana, V.; Lin, Q.; Pratt, D.; Kreyssig, A.; Ramazanoglu, M.; Corbett, J. D.; Goldman, A.; Miller, G. J. *Angew. Chem., Int. Ed.* **2012**, *51*, 12699−12702.
(7) Lin, Q.; Corbett, J. D. *Inorg. Chem.* **2008**, *47*, 7651−7659.
(8) Li, B.; Kim, S.-J.; Miller, G. J.; Corbett, J. D. *Inorg. Chem.* **2009**, *48*, 6573−6583.
(9) Mizutani, U. *Hume−Rothery Rules for Structurally Complex Alloy Phases*; CRC Press: Boca Raton, FL, 2011.
(10) *Chemistry, Structure and Bonding of Zintl Phases and Ions*; VCH Publishers: New York, 1996.
(11) Corbett, J. D. *Angew. Chem., Int. Ed.* **2000**, *39*, 670−690.
(12) Haucke, W. *Naturwissenschaften* **1937**, *25*, 61.
(13) Range, K. J.; Rau, F.; Klement, U. *Acta Crystallogr.* **1988**, *44*, 1485−1486.
(14) Zachwieja, U. *J. Alloys Compd.* **1996**, *235*, 12−14.
(15) Harms, W. *Atti Accad. Naz. Lincei, Cl. Sci. Fis., Mat. Nat., Rend.* **1970**, *48*, 235−241.
(16) Zachwieja, U. *J. Alloys Compd.* **1993**, *196*, 187−190.
(17) Raub, C. J.; Hamilton, D. C. *J. Less-Common Met.* **1964**, *6*, 486−488.
(18) Palenzona, A. *Atti Accad. Naz. Lincei, Cl. Sci. Fis., Mat. Nat., Rend.* **1967**, *42*, 504−509.
(19) Mueller, J.; Zachwieja, U. *Z. Anorg. Allg. Chem.* **2000**, *626*, 1867−1870.

(20) Smetana, V.; Miller, G. J.; Corbett, J. D. *Inorg. Chem.* **2013**, *52*, 12502−12510.
(21) Lin, Q.; Corbett, J. D. *J. Am. Chem. Soc.* **2012**, *134*, 4877−4884.
(22) Lin, Q.; Mishra, T.; Corbett, J. D. *J. Am. Chem. Soc.* **2013**, *135*, 11023−11031.
(23) Mishra, T.; Lin, Q.; Corbett, J. D. *Inorg. Chem.* **2013**, *52*, 13623−13630.
(24) Palasyuk, A.; Grin, Y.; Miller, G. J. *J. Am. Chem. Soc.* **2014**, *136*, 3108−3117.
(25) Smetana, V.; Corbett, J. D.; Miller, G. J. *Z. Anorg. Allg. Chem.* **2013**, *640*, 790−796.
(26) Pham, J.; Smetana, V.; Miller, G. J., manuscript in preparation.
(27) Ketelaar, J. *J. Chem. Phys.* **1937**, *5*, 668−668.
(28) Li, B.; Corbett, J. D. *Inorg. Chem.* **2007**, *46*, 6022−6028.
(29) *SMART*; Bruker AXS, Inc.: Madison, WI, 1996.
(30) Blessing, R. *Acta Crystallogr.* **1995**, *A51*, 33−38.
(31) Sheldrick, G. M. *SHELXS-97: Program for the solution of Crystal Structures*; University of Göttingen: Göttingen, Germany, 1997.
(32) Sheldrick, G. M. *Acta Crystallogr., Sect. A* **2008**, *64*, 112−122.
(33) Altomare, A.; Burla, M.; Camalli, M.; Carroccini, B.; Cascarano, G.; Giacovazzo, C.; Guagliardi, A.; Moliterni, A.; Polidori, G.; Rizzi, R. *J. Appl. Crystallogr.* **1999**, *32*, 115−119.
(34) Tank, R.; Jepsen, O.; Burkhardt, A.; Andersen, O. K. *TB-LMTO-ASA Program*, version 4.7; Max-Planck-Institut für Festkörperforschung: Stuttgart, Germany, 1994.
(35) Lambrecht, W. R. L.; Andersen, O. K. *Phys. Rev. B* **1986**, *34*, 2439−2449.
(36) Dronskowski, R.; Blöchl, P. E. *J. Phys. Chem.* **1993**, *97*, 8617−8624.
(37) Cordier, G.; Friedrich, T. *Z. Kristallogr.* **1992**, *201*, 308−309.
(38) Puselj, M.; Schubert, K. *J. Less-Common Met.* **1974**, *38*, 83−90.
(39) Bruzzone, G.; Ruggiero, A. F. *J. Less-Common Met.* **1964**, *7*, 368−372.
(40) Cordero, B.; Gomez, V.; Platero-Prats, A.; Reves, M.; Echeverria, J.; Cremades, E.; Barragan, F.; Alvarez, S. *Dalton Trans.* **2008**, *2008*, 2832−2838.
(41) Haarmann, F.; Prots, Y.; Goebel, S.; von Schnering, H. G. *Z. Kristallogr.* **2006**, *221*, 257−258.
(42) Sichevych, O.; Prots, Y.; Grin, Y. *Z. Kristallogr.* **2006**, *221*, 265−266.
(43) Palenzona, A. *J. Less-Common Met.* **1984**, *100*, 135−140.
(44) Tillard-Charbonnel, M.; Belin, C.; Soubeyroux, J. L. *Eur. J. Solid State Inorg. Chem.* **1990**, *27*, 759−769.
(45) Li, B.; Corbett, J. D. *J. Am. Chem. Soc.* **2005**, *127*, 926−932.
(46) Wu, Y.; Tenga, A.; Lidin, S.; Haeussermann, U. *J. Solid State Chem.* **2010**, *183*, 1574−1581.